Ocean Response to Surface Heat Anomalies

XINGJIAN JIANG

Department of Applied Physics, Columbia University and NASA/Goddard Institute for Space Studies, New York, New York

INEZ FUNG*

NASA/Goddard Institute for Space Studies, New York, New York

(Manuscript received 6 July 1993, in final form 10 October 1993)

ABSTRACT

An ocean general circulation model (OGCM) is used to study the response of ocean heat and mass transport to positive and negative heat flux anomalies at the ocean surface. As expected, tropical and low-latitude mixed layers respond rapidly (*e*-folding time about 50–70 years) to external forcing, while the response of the high-latitude mixed layer, especially the Southern Ocean and northern North Atlantic, is very slow (*e*-folding time greater than 300 yr). The overall response is faster for negative than positive heat flux anomaly at the surface. The meridional heat transport changes by 15% in the first 50 yr in the southern high latitudes. Surprisingly, for the next 400–500 yr the change is very small. The analysis shows that the meridional mass transport intensifies in response to a negative surface heat flux anomaly but weakens in response to a positive heat flux anomaly. For example, at model year 100 the NADW is reduced from about 18 Sv to about 10 Sv for the positive heat flux experiment but increased to about 26 Sv for the negative heat flux experiment.

1. Introduction

For a given climate forcing the equilibrium climate response is determined to a large extent by the magnitude of feedbacks in the climate system. The rate of approach to the equilibrium, or amount of realized climate change at any moment in time, is determined by the ocean.

In a series of calculations of transient climate change resulting from CO_2 increases using ocean GCMs and coupled atmosphere–ocean GCMs (Bryan et al. 1982, 1988; Washington and Meehl 1989; and Manabe et al. 1990, 1991) it is found that sea surface temperature (SST) warming proceeds at different paces at different latitudes, and is slower at high-latitude sinking regions.

Many models used in calculations of transient climate change employ simple treatments of the ocean's role in transient climate change, which ignore dynamical feedbacks between climate and ocean circulation (e.g., Hoffert et al. 1980; Hansen et al. 1984; Harvey and Schneider 1985). Meridional heat transport in the ocean is specified and assumed to remain unchanged in climate change in 100 years or so. Transports of heat perturbations, that is, departures from the model climatology, are treated as diffusive processes.

Such a simple ocean treatment, sometimes referred to as the "Q flux method," is used in the calculation of transient climate change using the GISS GCM (Hansen et al. 1988) and is now commonly used in several GCM calculations. Bryan et al. (1984) showed that for a constant surface perturbation of +0.5°C, a mixed-layer diffusive model yields, in terms of global averages, a fair global approximation of the penetration of the anomaly in both time and depth compared to an ocean GCM. The finding does not extend to a negative heat anomaly of −0.5°C, since the enhancement of convective overturning in high latitudes alters the vertical mixing rate in the ocean interior. This study addresses the response of positive and negative anomalies for a much larger perturbation.

In this study, we use an ocean GCM to estimate the variability of ocean heat and mass transports in a changing climate.

2. Model description and design of experiments

We use a version of the Bryan–Cox–Semtner ocean general circulation model (Bryan 1969; Bryan and Cox 1972; Bryan and Lewis 1979; Semtner 1974; and Cox 1984) recoded at GISS without modification of the physics and numerics of the original model. The recoding allows the code to run more efficiently on a dedicated IBM 560 workstation. The computational domain is global with realistic geometry and bottom

* Current affiliation: School of Earth and Ocean Sciences, University of Victoria, British Columbia, Canada.

Corresponding author address: Dr. Xingjian Jiang, NASA/GISS, 2880 Broadway, New York, NY 10025.

topography. The horizontal resolution is 4 degrees latitude by 5 degrees longitude. The ocean extends to a maximum depth of 4360 meters and is divided into 16 vertical layers, with layer thicknesses of 30, 60, 90, 120, 150, 180, 210, 240, 270, 310, 350, 390, 430, 470, 510, and 550 m. The choice of the 16 layers represents a compromise between computational economy and the need to keep numerical diffusivity below that of physical diffusivity in the model (Yin and Fung 1991). The horizontal and vertical momentum viscosities are chosen as 4×10^9 cm^2 s^{-1} and 20 cm^2 s^{-1}, respectively. The horizontal and vertical heat (and salt) diffusivities are $0.5 \times 10^7[1 + \exp(-z/500)]$ cm^2 s^{-1} and $0.8 + 1.05\{tg^{-1}[0.0045(z - 2500)]\}/\pi$ cm^2 s^{-1}, where z is the ocean depth in meters (Bryan and Lewis 1979).

The OGCM described above is first initialized from a state of rest with temperatures and salinities from the annual climatology of Levitus (1983). The model is forced at the surface by annual mean wind stresses from Hellerman and Rosenstein (1983). Surface mixed-layer temperature and salinity are restored (with a relaxation constant of 30 d^{-1}) to their observed annual mean values. The model is integrated for 9500 yr, at which time there is little trend in temperature, salinity, and velocity fields. The apparent heat and salt fluxes (Q_h and Q_s) are deduced from the last 800 yr of integration, and used as upper boundary conditions to the model for another 1000 yr, at the end of which, little trend in temperature, salinity, and velocity fields is found. All integrations, experiment and control, are started from the end of this run and integrated forward for 500 yr. The control is the extension of the run using the diagnosed Q_h and Q_s.

Several experiments are carried out where the upper boundary conditions are modified with heat flux anomalies (ΔQ_h) added to the surface thermal forcing field (Q_h). The freshwater fluxes and wind stress are the same as in the control integration. Hansen et al. (1984, 1985) have shown that as a first-order approximation, the surface air–sea heat flux anomaly can be written as

$$\Delta Q(\chi, t) = \frac{\Delta Q_{eq}[\Delta T_{eq} - \Delta T(\chi, t)]}{|\Delta T_{eq}|}, \qquad (1)$$

where ΔQ_{eq} is the equilibrium air–sea net heat flux change due to the atmospheric external forcing, and ΔT_{eq} is the corresponding equilibrium temperature change; $\Delta T(\chi, t)$ is the instantaneous temperature difference between the experiment and control integration in the mixed layer as the ocean approaches the equilibrium, and χ is the two-dimensional vector. For the present study ΔQ_{eq} is chosen to be 4 W m^{-2}, and ΔT_{eq} equals 4°, 2°, −2°, and −4°C, so that experiments are designated as P4, P2, N2, and N4, respectively. The value of $\Delta Q_{eq} = 4$ W m^{-2} and $\Delta T_{eq} = 4$°C correspond to $2 \times CO_2$ equilibrium climate change using the GISS GCM (Hansen et al. 1984). In this construct, the equilibrium temperature change for the mixed layer at different locations need not be the same as the global average (ΔT_{eq}). The experiments are thus designed to focus on the oceanic processes that contribute to the geographic variations of the mixed-layer response. Experiment P4 is similar to that in Hansen et al. (1984, 1985) and serves as the benchmark for comparing the results from simple ocean treatments with fixed horizontal heat transports.

We carry out two treatments of surface heat flux in regions of polar ice. The first ignores ice cover, so that the CO_2-induced air–sea heat flux is applied everywhere, while the second applies the heat flux anomaly only when the mixed-layer temperature is above −1.96°C, the freezing temperature of sea ice. The two cases represent bounds on the amount of heat flux penetrating beneath the sea ice. It turns out that these two treatments have insignificant impact on surface response time and heat and mass transports. Therefore, we shall focus on results from the first case, that is, ignore the existence of sea ice. We also focus on the P4 and N4 cases because of the similar oceanic response for P2 and N2.

Before discussing the results from experiments, we briefly describe the circulation in the control integration. The simulated temperature and salinity fields are in fair agreement with the observation of Levitus (1983). However, as has been found for other GFDL OGCM experiments (e.g., Toggweiler et al. 1989), the simulated thermocline seems too deep and too diffusive, especially in the equatorial region. As a whole, the ocean is relatively warmer and fresher than that observed. The model-simulated heat transport is in good agreement with Hsiung et al. (1989) but weaker than that reported by Oort and Vonder Haar (1976). The simulated meridional mass transport clearly shows the global-scale thermohaline circulations as proposed by Gordon (1986) and Broecker (1991).

3. Time scale analysis

In this section we discuss the ocean temperature response to the disturbance of thermal forcing by both positive and negative surface heat flux anomalies. The time evolution of global mean temperature anomaly at different depths for P4 and N4 experiments is shown in Fig. 1. At the end of year 500 the mixed-layer warming is about 3.26°C (and the cooling is about −3.46°C). The warming (cooling) of the bottom layer (4085 m) is about 0.92°C (−0.55°C).

The mixed layer shows a very rapid temperature change for the first 40–50 yr. The response then slows down and follows the change in deep layers. Below the mixed layer the ocean shows that the warming (or cooling) is continuous at an (almost) constant pace, with larger warming (or cooling) in the middle ocean and less warming (or cooling) in the deep ocean. Figure 1 also shows that positive anomalies penetrate much

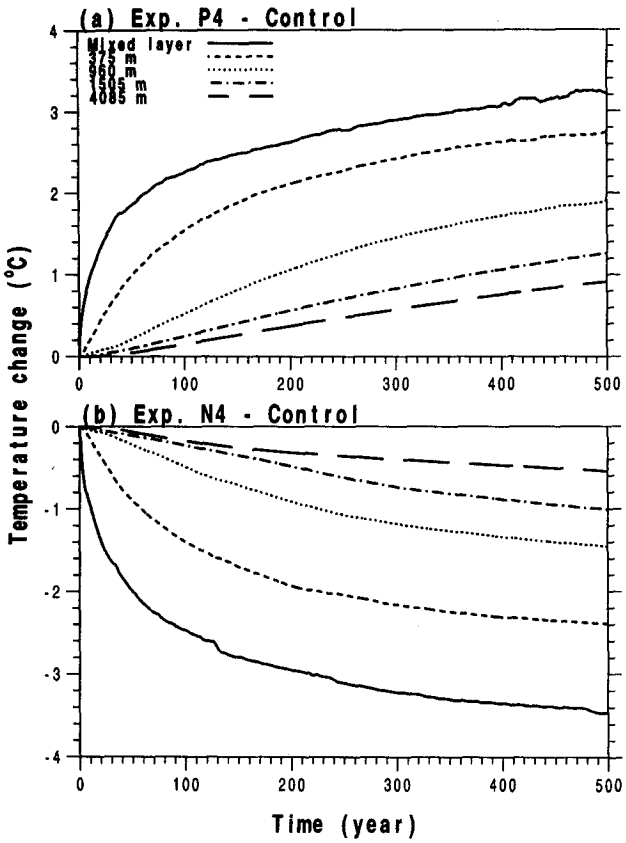

FIG. 1. Time evolution of globally averaged temperature differences (°C) between integrations (a) experiment P4 and control, and (b) experiment N4 and control at different depths.

deeper than negative anomalies, for example, the global mean warming of P4 is about 0.92°C at bottom ocean in year 500, while the cooling of N4 is only about −0.55°C.

Figure 2 shows the time evolution of the zonal mean temperature change of the surface mixed layer for experiments P4 and N4. In both experiments, the rapid response of the low and middle latitudes is clearly evident. The striking feature of the response for the experiment P4 is that large cooling occurs in the southern high latitudes, and the cooling persists throughout the 500 yr of model simulation near 60°S. The lower panel (experiment N4) shows very similar response except the warming in southern high latitudes is much smaller in magnitude than the cooling for P4. We will discuss the physical mechanisms that control the southern high-latitude cooling (warming) for P4 (N4) in section 4.

Hansen et al. (1985) showed that the surface response time is strongly dependent upon climate sensitivity, with larger sensitivity associated with slower response time and vice versa. Table 1 shows, from the OGCM results, time scales for the surface mixed layer to reach its equilibrium temperature for different climate sensitivities. Results are shown for the experiments with and without polar ice cover as well as for the mixed-layer diffusive ocean model used in Hansen et al. (1984). The time for the global mean mixed-layer temperature to reach 50% and 63% (e-folding) of its equilibrium temperature change is about 63 and 165 yr, respectively, for experiment P4, and about 51 and 110 yr, respectively, for experiment N4. This result is consistent with other model studies (Schlesinger et al. 1985; Bryan et al. 1988; Schlesinger and Jiang 1990; and Manabe et al. 1990), taking into account the different climate sensitivities of the various models. The result of experiment P4 is similar to that of Hansen et al. (1984), whose mixed-layer diffusive ocean with fixed horizontal heat transports gives a surface e-folding time of about 139 years for the same ΔT_{eq} and ΔQ_{eq}. The 3D model results also confirm that the surface response time is faster when the climate sensitivity is smaller. As expected, the e-folding time is a little bit longer when polar sea ice is included. With the mixed-layer diffusive ocean model, the response is symmetric

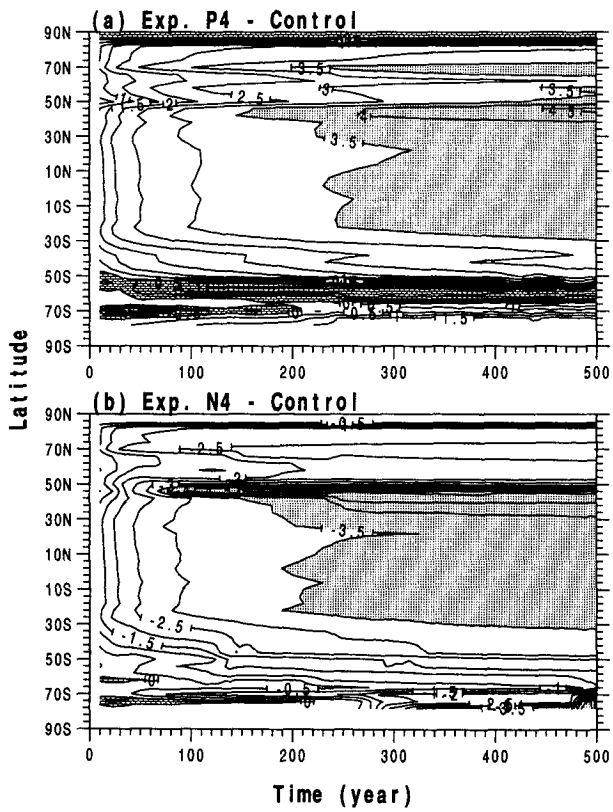

FIG. 2. Time evolution of the zonally averaged mixed-layer temperature difference (°C) between the integrations (a) experiment P4 and control (dotted shading indicates values larger than 3.5°C and brick shading for values less than 0°C), and (b) experiment N4 and control (dotted shading indicates values less than −3.5°C and brick shading for values larger than 0°C).

for positive and negative surface heat anomalies. The longer response time of P4 than that of N4 is consistent with the result shown by Bryan et al. (1984). As we will see later it is the Southern Ocean that makes the difference between experiment P4 and N4.

Figure 3 shows the geographical distribution of the mixed-layer *e*-folding response time for experiments P4 and N4. Global mean equilibrium temperature, ΔT_{eq}, is assumed everywhere. The response time in low latitudes is around 50–75 yr, only half that of the global mean value, while the response time in the high latitudes, especially in the northern North Atlantic and the circumpolar oceanic latitudes, exceeds 300 yr. Hansen et al. (1984) showed very similar results, even though their calculation completely neglected the dynamical response of the ocean circulation. Between the two experiments, there is very little difference in *e*-folding times in the low latitude but there are significant differences in high latitudes. For example, the northern North Pacific has an *e*-folding time of 300 yr for experiment P4 but 75 years for experiment N4. The overall response in the southern high latitudes is shorter by 80 years for negative heat flux anomaly than for positive heat flux anomaly. Using a coupled atmosphere–ocean GCM, Manabe et al. (1990, 1991) also found that the response of tropical surface ocean is much faster than that in the high latitudes. The minimum response occurred in the deep water formation region of their model, especially near the antarctic coast where large cooling (or warming) was found for the increase (or decrease) of atmospheric CO_2.

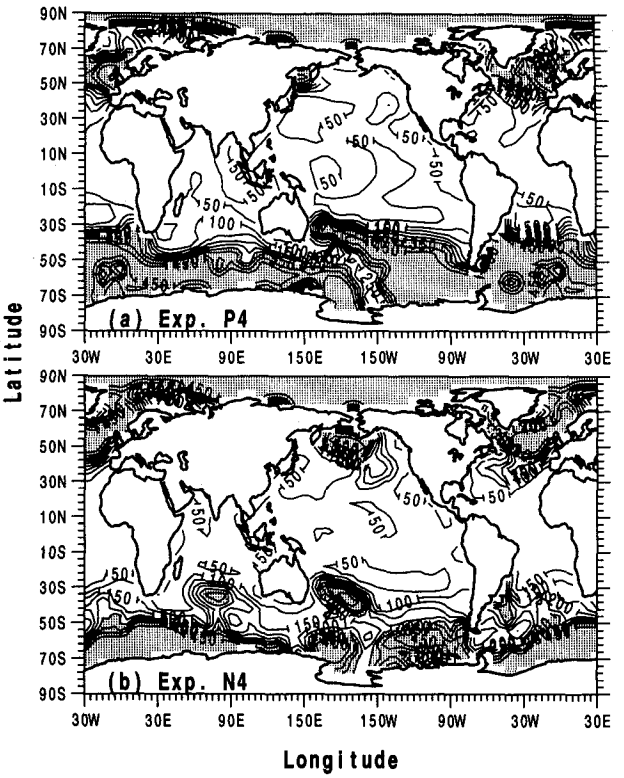

FIG. 3. Geographical distribution of the *e*-folding response time (years) for the surface mixed-layer temperature in response to surface (a) positive heat flux anomaly, and (b) negative heat flux anomaly. The equilibrium temperature is uniform everywhere at 4°C for experiment P4 and −4°C for experiment N4, respectively. Areas with value larger than 300 yr are shaded.

4. Heat and mass transport analysis

In this section we focus on the response of ocean heat and mass transports to the surface heat flux anomalies, and their relative contribution to the surface temperature trends.

Figure 4 shows the zonally and vertically integrated meridional heat transport for the control run and for the differences between experiment and control at years 50, 100, 200, and 400 of the integration. The heat transport of the control run is close to the observed value derived by Hsiung et al. (1989) and to modeling studies, for example, Manabe et al. (1990, 1991) and England (1993), but is slightly underestimated compared to other observation-derived transports, for example, Oort and Vonder Haar (1976) and Hastenrath (1980). Poleward heat transports are found for both

TABLE 1. Time (year) needed to reach 50%, 63% (the *e*-folding time), and 75% of the equilibrium temperature change of the mixed layer for different experiments.

		Experiment P4 (ΔT_{eq} = 4°C)	Experiment P2 (ΔT_{eq} = 2°C)	Experiment N2 (ΔT_{eq} = −2°C)	Experiment N4 (ΔT_{eq} = −4°C)
No ice cover	50%	63	23	19	51
	e-folding	165	70	42	110
	75%	356	193	79	218
With ice cover	50%	49	22	21	51
	e-folding	166	46	48	112
	75%	443	227	103	237
Pure diffusion model	50%	54	17	17	54
	e-folding	139	40	40	139
	75%	336	103	103	336

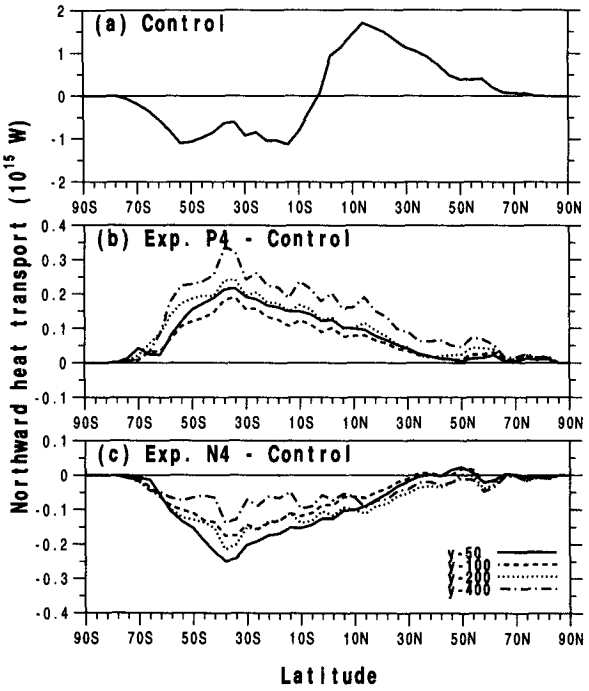

FIG. 4. Zonally and vertically integrated northward heat transport (10^{15} W) for (a) the control integration, (b) difference between experiment P4 and control, and (c) difference between experiment N4 and control at model years 50, 100, 200, and 400.

experiments at all times. Compared to the control experiment, poleward heat transport is intensified for experiment N4 and weakened for experiment P4 in the Southern Hemisphere, especially between 10°S and 60°S where 10%–20% change is observed for both experiments in all the simulation years. Northern Hemispheric heat transports are practically constant for both P4 and N4 in the 500 years of the simulation. It is interesting to note that as the experiments continue the weakening of the southern high-latitude southward heat transport in P4 is getting larger, while the strengthening of the heat transport in N4 is getting smaller. The direct consequence of weakening southward heat transport in P4 is the cooling of the upper ocean. This cooling would enhance convective overturning and effectively transport surface heat anomaly to the deep ocean. As shown later in Fig. 5 the change of meridional heat transport due to the thermal response cannot compensate for the opposite role by the dynamical response, and the southward heat transport is further weakened. Thus, for the positive heat flux experiment both the convection and meridional heat transport processes tend to delay the surface response time. For experiment N4 the intensified southward heat transport causes warming in the upper ocean and delays the surface response. This warming would reduce the convective overturning, however, and less effectively transport the heat anomaly to deep ocean. Thus, for the negative heat flux experiment, convective overturning and meridional heat transport play opposite roles. The changes of the meridional heat transport from year to year shown in Fig. 4 support this argument. As we will see later the change of meridional heat transport is critical in maintaining the southern high-latitude cooling (warming) for experiment P4 (N4). The changes of heat transport in the Southern Hemisphere for both P4 and N4 are similar to those reported by Manabe et al. (1991) for years 60–80 of their coupled models with 1% increase or decrease of atmospheric CO_2 concentration. The changes in the Northern Hemisphere here are smaller than those of Manabe et al. (1991), however.

To further understand the response of the meridional heat transport we express (V, T), the instantaneous velocities and temperatures from the experiments as departures $(\Delta V, \Delta T)$ from (V^*, T^*), the corresponding mean values from control run:

$$V(t) = V^* + \Delta V(t) \text{ and } T(t) = T^* + \Delta T(t). \quad (2)$$

The meridional heat transport for the experimental integration can be written as

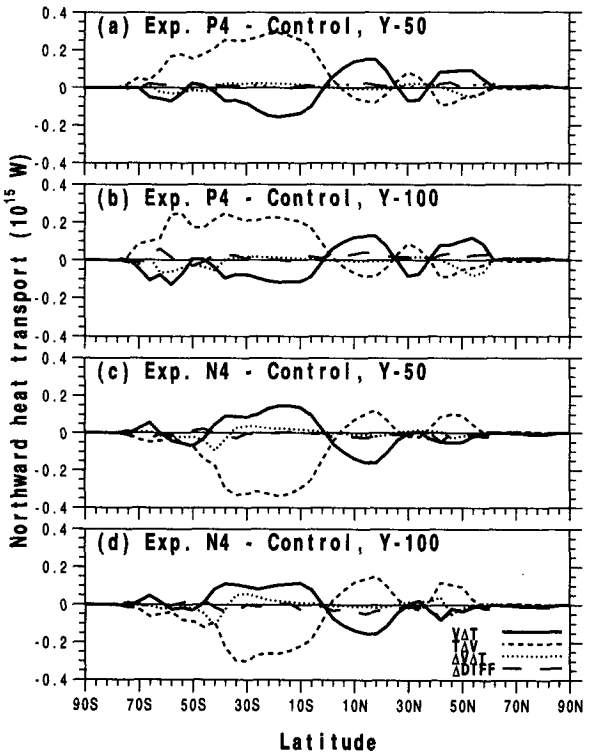

FIG. 5. Zonally and vertically integrated northward heat transport (10^{15} W) for the individual component of the last four terms on the rhs of Eq. (3) for [(a) and (b)] positive heat flux experiment, and [(c) and (d)] negative heat flux experiment at years 50 and 100.

$$\int_0^{2\pi}\int_{-D}^{0}\left(VT - A_H\frac{\partial T}{\partial\phi}\right)a\cos\phi d\lambda dz$$
$$= \int_0^{2\pi}\int_{-D}^{0}\left(V^*T^* - A_H\frac{\partial T^*}{\partial\phi}\right)a\cos\phi d\lambda dz$$
$$+ \int_0^{2\pi}\int_{-D}^{0}\left(V^*\Delta T + T^*\Delta V + \Delta V\Delta T - A_H\frac{\partial\Delta T}{\partial\phi}\right)a\cos\phi d\lambda dz. \quad (3)$$

The first two terms on the right-hand side of Eq. (3) represent the meridional heat transport from control integration, the next four terms are the differences between the experiment and control integration.

The zonally and vertically integrated values of the last four terms of Eq. (3) are shown in Fig. 5 for experiments P4 and N4 at years 50 and 100 (other years show very similar structures). There is a large compensation between $V^*\Delta T$ and $T^*\Delta V$, that is, the transport of the thermal anomaly by mean currents and the transport of mean temperatures by velocity anomalies in most latitudes except between 10°S and 60°S where $T^*\Delta V$ cannot be compensated. The higher-order terms, $\Delta V\Delta T$ and $-A_H(\partial\Delta T/\partial y)$, only play a minor role. For the positive flux anomaly experiment, $V^*\Delta T$ acts to intensify the total northward heat transport, while $T^*\Delta V$ acts to weaken the total northward heat transport. For the negative flux anomaly experiment, however, the two terms play the opposite role in weakening or intensifying northward heat transport. Figure 5 shows that the insensitivity of the meridional heat transport in the Northern Hemisphere is due to the compensation between terms of $V^*\Delta T$ and $T^*\Delta V$. But in the Southern Hemisphere these two terms cannot balance each other because of the small change of ΔT (as shown in Fig. 2) in the southern middle and high latitudes. The hemispheric difference in high-latitude response of upper-layer temperature results in large asymmetric heat transport changes for the two hemispheres. Manabe et al. (1990) argued that the decrease of southward heat transport was caused by the intensification of equatorward Ekman drift, resulting from the increase of surface westerlies. The present study indicates that the reduction of southward heat flux is the direct consequence of slow warming in the southern upper ocean. The role of the $T^*\Delta V$ term in the total heat transport suggests that V is decreased for the positive surface heat flux anomaly experiment and increased for the negative surface heat flux anomaly experiment, as will be shown next.

The meridional mass transport of the global ocean for the control integration and the differences between experiment and control integration at year 100 are shown in Fig. 6. The mass transport of the control experiment (top panel) clearly shows the conveyor belt discussed by Gordon (1986) and Broecker (1991) with

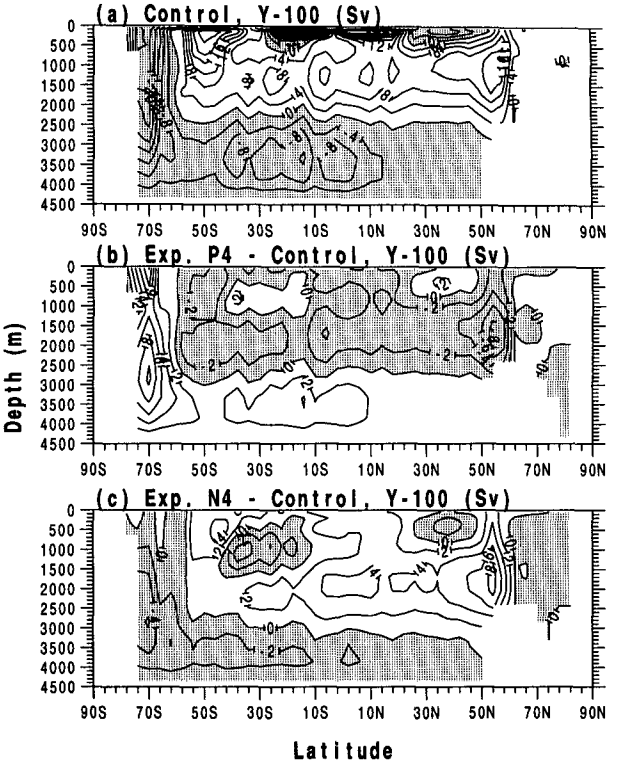

FIG. 6. The latitude–depth distribution of the meridional mass streamfunction (Sv) over all oceans at model year 100 for (a) the control integration, (b) experiment P4 minus control, and (c) experiment N4 minus control. Negative values are shaded.

the circulation cells of the North Atlantic Deep Water (NADW) and the Antarctic Bottom Water (AABW). The magnitudes of the NADW and AABW are about 18 Sv and 25 Sv, respectively. The wind-driven cells are confined in the upper 1000 m. In experiment P4 the meridional circulation is weaker almost everywhere compared to the control experiment (middle panel). The largest reduction of the thermohaline circulation occurs near 60°N and the Antarctic continent, with maximum decreases of 8 and 8 Sv, respectively. The lowest panel of Fig. 6 shows that the thermohaline circulation is intensified for the negative heat flux anomaly experiment. The magnitudes of change for N4 and P4 are comparable. Figure 6 also shows very small change in the meridional streamfunction near the sea surface because of the same wind stress field being used for both experiment and control integrations. Similar responses of the meridional circulation are also found by Bryan et al. (1988) and Manabe et al. (1990, 1991).

In section 3 we have seen that the surface response of southern high latitudes behaves very differently from other latitudes for both P4 and N4 experiments. Cooling (warming) is found in certain latitudes during the transient evolution for experiment P4 (N4). The magnitude of the cooling for P4 is much stronger than the warming for N4, however. Manabe et al. (1990, 1991)

showed very similar results for increase or decrease of atmospheric CO_2 concentration, except their warming for decrease of CO_2 is larger in magnitude than the cooling for increase of CO_2. In their 1990 paper, Manabe et al. argued that the cooling of the southern high latitudes is due to the reduction of upper-layer convection caused by the decrease of surface salinity. In the present study, however, the surface freshwater flux is the same for control and experiment integrations, hence, the surface salinity plays no role in reducing the convective activity. In the following we analyze the contributions of the individual physical processes to the surface mixed-layer temperature change in the southern high latitudes. The total (net) change is broken down to changes due to surface heating, vertical convection, meridional advection, vertical advection and others, including east–west advection and all eddy diffusion terms. Figure 7 shows the difference in these components between the experiment and the control as averaged over years 50–70 of the experiment for the southern high latitudes. For experiment P4, larger cooling rates occur near 54°S and 70°S. The surface heating anomaly always warms up the mixed layer. The decrease in vertical convection, however, results in reduced warming, that is, cooling of the surface mixed layer. The weaker southward heat transport also tends to cool the surface mixed layer except in a few narrow latitudinal bands. All other terms only play a secondary role. So it is the reduced convection and meridional heat transport that sustain the cooling near 50°S and 70°S.

This result is consistent with that shown by Bryan et al. (1988) and Manabe et al. (1990). In the present study, however, the cooling effect of the meridional heat transport is stronger, and the mechanism of reducing convective overturning is different. It is the reduced strength of convection that gives overall convective cooling as shown in Fig. 7, because the whole depth of the water column has been already well ventilated. In contrast to the strength, the frequency of convection actually increased for P4 compared with control integration, due to the persistent cooling. This argument is supported by the heat anomaly distribution in the bottom ocean layer where large warming is found in the low and middle latitudes. Thus for experiment P4, the heat anomaly entering southern high latitudes is rapidly transported to the deep ocean through vertical mixing processes. There it is carried out of the southern deep ocean by the (weaker) AABW to middle- and low-latitude deep ocean and eventually returns to the surface through the low-latitude upwelling process.

In the context of 1D box-diffusion models, it is often argued (e.g., Schneider and Thompson 1981) that surface heating would increase the stratification of the water column, decouple the upper ocean from the interior, and accelerate the surface response time. Our conclusions from the 3D model experiment are contrary due to the dynamical response of the meridional heat transport.

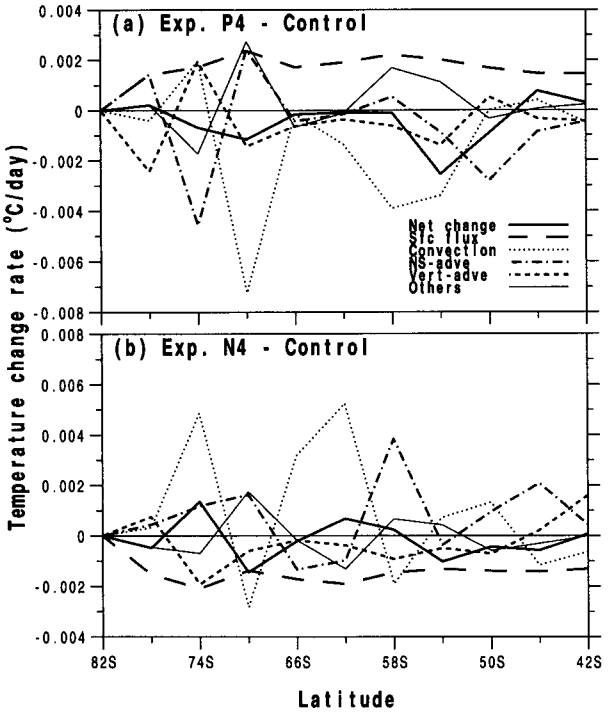

FIG. 7. Zonal mean southern high-latitude mixed-layer temperature change rate (°C day^{-1}) due to surface heating, convective overturning, meridional and vertical advection, and all other processes averaged over model years 50–70 for the difference between (a) experiment P4 and control, and (b) experiment N4 and control.

The bottom panel of Fig. 7 for experiment N4 shows a similar but opposite situation, except that the magnitude of the warming rate is relatively small. Thus it is the suppressed (intensified) convective overturning plus the reduced (increased) southward heat transport that causes the southern high latitudes to respond faster for N4 than for P4.

5. Discussion and summary

An ocean general circulation model is used to study the response of ocean heat and mass transports to positive and negative heat flux anomalies at the surface. The specification of surface heat flux anomalies [Eq. (1)] simply represents a first-order approximation to the actual heat flux (Hansen et al. 1984). Nevertheless, the latitudinal distribution of the anomalies is very similar to that directly computed from coupled atmosphere–ocean GCMs (e.g., Schlesinger and Jiang 1988; Manabe et al. 1990, 1991). The specification, however, does not permit feedbacks through the atmosphere, which has a much shorter response time to thermal perturbations than the ocean. Thus our study effectively isolates the oceanic response to the flux anomalies and investigates the oceanic processes that

explain the response. While we make comparisons with results from coupled model runs in our analysis, it is difficult at the moment to evaluate the relative roles played by the atmosphere and the ocean without a parallel analysis of a coupled experiment.

It is found that the tropical and low-latitudinal ocean respond faster, by as much as a factor of 5, than the high-latitude ocean, especially the Southern Ocean and northern North Atlantic. This result is consistent with studies of Hansen et al. (1984, 1985) who used a mixed-layer diffusive ocean model and Manabe et al. (1991) who used a coupled atmosphere–ocean GCM. The *e*-folding time of the global mean surface temperature due to the surface heating is about 165 yr for $\Delta T_{eq} = 4°C$ and 70 yr for $\Delta T_{eq} = 2°C$. For the negative heat flux anomaly the *e*-folding time is shorter: about 110 yr for $\Delta T_{eq} = -4°C$ and 42 yr for $\Delta T_{eq} = -2°C$.

The largest change of meridional heat transport is about 15% and occurs in the first 50 years between 10°S and 50°S, where southward transport weakens for the positive heat flux experiment and intensifies for the negative heat flux experiment. Surprisingly, over the next 450 yr no further change occurred in response to the surface heat flux anomaly. The insensitivity of the meridional heat transport is caused by the compensating roles of weakened (strengthened) meridional mass transport and stronger (weaker) upper-ocean temperature gradients in response to the penetration of positive (negative) heat anomalies.

The changes in thermohaline circulation in the present study are consistent with those in other studies. At year 100, the NADW is reduced from about 18 Sv to about 10 Sv for experiment P4, but increased to about 26 Sv for experiment N4. This symmetric response of NADW might be due to the deliberate exclusion of salinity effects in the experiments. The response is expected to be quite different in a fully coupled model since salinity plays such a dominant role in the very high latitudes.

The relative small change of the meridional heat transport for a large portion of ocean over 500 years appears to support the assumption necessitated in GCM studies that employ simplified treatments of the ocean (e.g., Hansen et al. 1988). The OGCM results highlight that there is important physics not included in the simple models, however. In particular, convective overturning plays a dominant role in the heat budget of the high-latitude surface oceans, and changes in its magnitude and frequency are responsible for the asymmetry of the response times between positive and negative heat flux anomalies, and the opposite surface temperature response in the sinking regions compared to the rest of the ocean.

Manabe et al. (1991) argued, in their coupled model study of the response to changing atmospheric CO_2 concentration, that the changes in surface wind stress and surface salinity might be the driving force of the increase or decrease of the thermohaline circulation. The present study indicates that in the absence of these changes in forcing, anomalies in the thermal field can induce qualitatively similar change in the thermohaline circulation, however.

Acknowledgments. We thank Dr. J. E. Hansen for stimulating this research and the anonymous reviewers for helpful comments. The support of NASA Earth System Modeling and Global Analysis Branch is gratefully acknowledged. XJ is a NOAA Post-doctoral Fellow resident at GISS.

REFERENCES

Broecker, W. S., 1991: The great ocean conveyor. *Oceanogr.*, **4,** 79–89.

Bryan, K., 1969: Climate and the ocean circulation. III: The ocean model. *Mon. Wea. Rev.*, **97,** 806–827.

——, and M. D. Cox, 1972: An approximate equation of state for numerical model of ocean circulation. *J. Phys. Oceanogr.*, **2,** 510–514.

——, and L. J. Lewis, 1979: A water mass model of the World Ocean. *J. Geophys. Res.*, **84,** 2503–2517.

——, F. G. Komro, S. Manabe, and M. J. Spelman, 1982: Transient climate response to increase atmospheric carbon dioxide. *Science,* **215,** 56–58.

——, ——, and C. Rooth, 1984: The ocean's transient response to global surface temperature anomalies. *Climate Processes and Climate Sensitivity,* Geophys. Monogr., No. 29, Maurice Ewing, Vol. 5, J. E. Hansen, and T. Takahashi, Eds., Amer. Geophys. Union, 29–38.

——, S. Manabe, and M. J. Spelman, 1988: Interhemispheric asymmetry in the transient response of a coupled ocean-atmospheric model to a CO_2 forcing. *J. Phys. Oceanogr.*, **18,** 851–867.

Cox, M. D., 1984: A primitive equation, three-dimensional model of the ocean. GFDL Ocean Group Tech. Rep. No. 1, GFDL, Princeton University, 143 pp. [Available from Princeton University, Princeton, NJ.]

England, M. H., 1993: Representing the global-scale water masses in ocean general circulation models. *J. Phys. Oceanogr.*, **23,** 1523–1552.

Gordon, A. L., 1986: Interocean exchange of thermocline water. *J. Geophys. Res.*, **91,** 5037–5046.

Hansen, J., A. Lacis, D. Rind, G. Russell, and P. Stone, 1984: Climate sensitivity: Analysis of feedback mechanism. *Climate Processes and Climate Sensitivity,* Geophys. Monogr., No. 29, Maurice Ewing, Vol. 5, J. E. Hansen and T. Takahashi, Eds., Amer. Geophys. Union, 130–163.

——, G. Russell, A. Lacis, I. Fung, D. Rind, and P. Stone, 1985: Climate response times: Dependence on climate sensitivity and ocean mixing. *Sciences,* **229,** 857–859.

——, I. Fung, A. Lacis, D. Rind, S. Lebedeff, R. Ruedy, and G. Russell, 1988: Global Climate changes as forecast by the Goddard Institute for Space Sciences three dimensional model. *J. Geophys. Res.*, **93,** 9341–9364.

Harvey, L. D., and S. Schneider, 1985: Transient climate response to external forcing on 10^0–10^4 year time scales. Part I: Experiment with globally averaged, coupled atmosphere and ocean energy balance model. *J. Geophys. Res.*, **90,** 2191–2205.

Hastenrath, S., 1980: Heat budget of tropical ocean and atmosphere. *J. Phys. Oceanogr.*, **10,** 159–170.

Hellerman, S., and M. Rosenstein, 1983: Normal monthly wind stress over the World Ocean with error estimates. *J. Phys. Oceanogr.*, **13,** 1093–1104.

Hoffert, M. I., A. J. Callegari, and C.-T. Hsieh, 1980: The role of deep sea storage in the secular response to climate forcing. *J. Geophys. Res.*, **85,** 6667–6679.

Hsiung, J., R. E. Newell, and T. Houghtby, 1989: The annual cycle of oceanic heat storage and oceanic meridional heat transport. *Quart. J. Roy. Meteor. Soc.*, **115,** 1–28.

Levitus, S., 1983: *Climatological Atlas of the World Ocean.* NOAA Prof. Paper 13, U.S. Dept. of Commerce, 173 pp. [Available from U.S. Department of Commerce, Washington, D.C.]

Manabe, S., K. Bryan, and M. J. Spelman, 1990: Transient response of a global ocean–atmosphere model to a doubling of atmospheric carbon dioxide. *J. Phys. Oceanogr.,* **20,** 722–749.

——, R. J. Stouffer, M. J. Spelman, and K. Bryan, 1991: Transient response of a coupled ocean-atmosphere model to gradual changes of atmospheric carbon dioxide. Part I: Annual mean response. *J. Climate,* **4,** 785–818.

Oort, A. H., and T. H. Vonder Haar, 1976: On the observed annual cycle in the ocean-atmosphere heat balance over the Northern Hemisphere. *J. Phys. Oceanogr.,* **6,** 781–800.

Schlesinger, M. E., and X. Jiang, 1988: The transport of CO_2-induced warming into the ocean: an analysis of simulations by the OSU coupled atmosphere-ocean general circulation model. *Climate Dyn.,* **3,** 1–17.

——, and ——, 1990: Simple model representation of atmosphere-ocean GCMs and estimation of the time scale of CO_2-induced climate change. *J. Climate,* **3,** 1297–1315.

——, W. L. Gates and Y. J. Han, 1985: The role of the ocean in CO_2-induced climatic warming: Preliminary results from the OSU coupled atmosphere-ocean GCM. *Coupled Ocean-Atmosphere Models,* J. C. J. Nihoul, Ed., Elsevier, 447–478.

Schneider, S. H., and S. L. Thompson, 1981: Atmospheric CO_2 and climate: Importance of the transient response. *J. Geophys. Res.,* **86,** 3135–3147.

Semtner, A. J., 1974: A general circulation model for the World Ocean. Tech. Rep. No. 8, 99 pp. [Available from University of California, Los Angeles, Department of Meteorology, Los Angeles, CA.]

Toggweiler, J. R., K. Dixon, and K. Bryan, 1989: Simulations of radiocarbon in a coarse-resolution world ocean model 1. Steady state prebomb distributions. *J. Geophys. Res.,* **94,** 8217–8242.

Washington, W. M., and G. A. Meehl, 1989: Climate sensitivity due to increase CO_2: Experiments with a coupled atmosphere and ocean general circulation model. *Climate Dyn.,* **4,** 1–38.

Yin, F. L., and I. Fung, 1991: Net diffusivity in ocean general circulation models with nonuniform grids. *J. Geophys. Res.,* **96,** 10 773–10 776.